Chemical Engineering Journal 381 (2020) 122639

Contents lists available at ScienceDirect

Chemical Engineering Journal

journal homepage: www.elsevier.com/locate/cej

Evaporation-condensation in the presence of unipolar ionic flow for solvent-free production of ultrasmall antibacterial particles

Dae Hoon Park[a], Yun Haeng Joe[b], Jungho Hwang[a,*], Jeong Hoon Byeon[c,*]

[a] School of Mechanical Engineering, Yonsei University, Seoul 03722, Republic of Korea
[b] Climate Change Research Division, Korea Institute of Energy Research, Daejeon 34129, Republic of Korea
[c] School of Mechanical Engineering, Yeungnam University, Gyeongsan 38541, Republic of Korea

HIGHLIGHTS

- The constant manufacture of ultrasmall particles was achieved by a solvent-free process.
- The ultrasmall particles provided more stable results in antibacterial activities.
- The solvent-free process offered precision antibacterials in a plug-in supply manner.

GRAPHICAL ABSTRACT

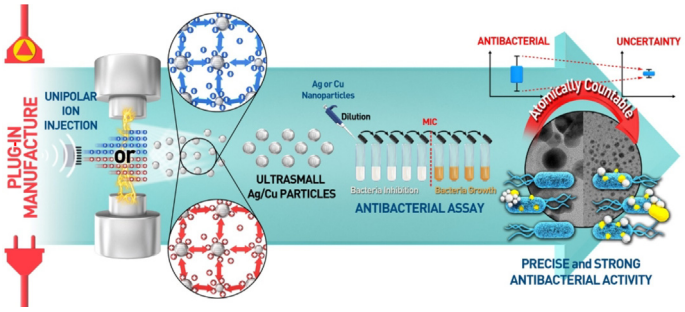

ARTICLE INFO

Keywords:
Antibiotic resistance
Antibacterial activity
Plug-in manufacture
Ultrasmall particles
Tandem electrostatic system

ABSTRACT

Because of antibiotic resistance threats, there has been a resurgence of interest in Ag or Cu nanoparticles (NPs) with soft functional components as composite particulates or coatings for broad-spectrum and strong antibacterials despite the biotoxicity of the NPs. Although the composite architectures conferred stimuli-responsive and safer antibacterial functions to the particulates or coatings, the renewal of antibacterial activity for long-term care remains a challenge, and the preparation and storage of the composites require complex and costly chemistries and procedures. Consequently, developing a digitizable platform for the plug-in manufacture of ultrasmall (atomically countable) Ag or Cu particles may represent an important advancement because an on-demand post-processing method for conferring functional overlayers onto NPs was recently introduced. In this study, a tandem electrostatic system consisting of a carbon brush ionizer and a spark ablation device was developed, in which gaseous ions (1×10^7 ions cm^{-3}) were injected into the spark ablation passage between Ag or Cu rods to ensure the steady and uniform manufacture of ultrasmall Ag or Cu particles (~3 nm). The resulting Ag or Cu particles exhibited stronger and more stable antibacterial activities against bacteria (including multidrug-resistant strains) than Ag or Cu NPs (> 10 nm).

1. Introduction

Bacterial attachment and subsequent growth on surfaces can induce serious problems in human healthcare, bioengineering, and bioindustry; thus, considerable research efforts have focused on the development of efficient antibacterial materials and processes [1–3]. Conversely, increases in antibacterial resistance to traditional antibiotics has necessitated the development of alternative materials with

* Corresponding authors.
E-mail addresses: hwangjh@yonsei.ac.kr (J. Hwang), postjb@yu.ac.kr (J.H. Byeon).

https://doi.org/10.1016/j.cej.2019.122639
Received 4 June 2019; Received in revised form 26 August 2019; Accepted 27 August 2019
Available online 28 August 2019
1385-8947/ © 2019 Elsevier B.V. All rights reserved.

long-term inhibitory activity against a broad spectrum of bacteria and microorganisms [4]. Although several biochemistries have been recently used to develop strong antibacterials for microbes, including multidrug-resistant (MDR) bacteria, the preparation and validation of a new class of the antibacterial materials require complex processes and time-consuming procedures, resulting in higher optimization and manufacturing costs [5,6].The applications of the materials also require various types of verification, suggesting that different approaches are simultaneously required to ensure the timely development of realizable antibacterials [7].

The use of inorganic (Ag, Cu, Zn, or Mg) nanoparticles (NPs, 10–100 nm) has emerged as a novel approach for scientific research as well as the development of antibacterial systems and strategies because of their qualified broad-spectrum activity and cost-effectiveness [8–11]. These NPs have diverse applications, such as water (both waste and drinking) treatment, biofouling prevention, and infectious disease treatment, including bacterial growth inhibition on various surfaces [12–15]. In particular, Ag or Cu NPs have been frequently used for these purposes, and their strong activity against a wide range of bacteria, including MDR strains, is probably attributable to the interaction between released $Ag+$ or $Cu2+$ ions from the NP surfaces and the membrane proteins of bacteria [8]. This interaction can cause deformation of the cell membrane and DNA, thereby disturbing cell metabolism and inhibiting bacterial replication [16]. Although the potential toxicities or side effects should be considered for their practical application, rationalizing the issues by incorporating hydrogel matrix-containing proteins, peptides, lipids, biomolecules, or synthetic polymers to form composite particulates, and coatings have been successfully reported in recent years [17,18].

The on-demand release of $Ag+$ from Ag NPs by incorporating stimuli-responsive compounds into the composite particulates and coatings to avoid faster release in the short term and antibacterial resistance is an emerging area of antibacterial research [19]. pH-, thermo-, opto-, magneto-, or sono-responsive composite architectures have been designed and evaluated for development of the on-demand and sustained antibacterials [20–24]. Hydrochemical approaches have generally been utilized to prepare composite materials composed of Ag NPs with finely tuned sizes and shapes; however, the preparation is usually based on multistep reactions with hazardous chemicals and complex controls [25,26], as well as limited ability to secure a digital dispensing system for on-site renewal of the antibacterial particulates or coatings [27]. Moreover, aggregation and hydrolysis (*i.e.*, altering the original properties) of finely tuned Ag NPs during storage are other challenges to the precise and sustained release of $Ag+$, although surface functionalization for achieving stimuli-responsive and biosafe properties can be rationalized *via* mechanical spraying onto Ag NPs [28] or the in-flight encapsulation of Ag NPs with functional molecules instead of hydrochemistries [29,30].

To this end, the plug-in manufacture of Ag or Cu NPs through plasma-induced evaporation-condensation or polymerization has been introduced to provide an effective platform for tunable and switchable antibacterial activities [31]. More recently, atmospheric pressure plasmas for NP manufacture have been developed to resolve issues regarding the cost and equipment size of vacuum plasmas; however, the much greater diffusion coefficients of the plasma-produced NPs in the gas phase (three orders greater than NPs in the aqueous phase) lead to rapid agglomeration (inducing larger sizes with nonuniform distributions) of primary (singlet) particles [32]. This implies that the precise and on-site renewal of antibacterial activity remains a major hurdle despite the availability of base technologies for the plug-in manufacture and on-site surface functionalization of antibacterial NPs. Developing a realizable compact platform to produce ultrasmall antibacterial NPs (*i.e.*, atomically countable sizes to ensure the precise release of ions from antibacterial NPs) is therefore essential for the low-cost and tunable fabrication of antibacterial particulates or coatings. Specifically, spherical face-centered cubic (fcc) particles (*e.g.*, Ag or Cu) smaller than 3.7 nm (consisting of < 100 atoms) are more suitable relative to the amount of active atoms, making them highly desirable for the precise and tunable release of antibacterial ions [33], as the size directly affects the atom numbers of NPs, including surface energy and chemical reactivity for strong antibacterial activities [34]. Furthermore, ultrasmall sizes are suitable for renal excretion to minimize systemic toxicities from NP exposure in patients [35].

In the present study, a plug-in system with the size of a business card was developed for the constant manufacture of ultrasmall Ag or Cu particles under gas flow to provide coherent and strong antibacterial activity. Co-installation of unipolar gas ionization and an atmospheric pressure spark ablation inside the device (32 [length] × 32 [height] × 32 [width] mm^3) increased the discharge coefficient (*C*d) of gas that passes through the spark channel (Fig. S1). A carbon-brush type ionizer (positive or negative) was used for the ionization of carrier gas, whereas two insulated gate bipolar transistor (IGBT) switches and a high-voltage direct current (DC) power supply were connected to two Ag or Cu rods (separated by 0.3 mm) for the ablation (Figs. S2A–S2C). By injecting positive or negative gaseous ions into the spark ablation channel, a stable current-time profile from electrostatically (positively or negatively) charged particles could be generated, unlike the configuration of the no-ion injection (Fig. S2D). This significantly reduced both the agglomeration of singlet Ag or Cu particles and the fluctuation of particle generation, resulting in the steady and uniform manufacture of ultrasmall Ag or Cu particles. Compared with hydrochemical synthesis, the use of a plug-in continuous gas flow system facilitated the on-demand supply of ultrasmall Ag or Cu particles from evaporation and subsequent unipolar charging of Ag or Cu metal (inducing condensation of Ag or Cu vapors as an electrostatically repulsive configuration to prevent aggregation between the vapors, as well as Brownian collision between singlet Ag or Cu particles), providing an effective compact tool for generating *in situ* ultrasmall Ag or Cu particles without the use of additive and stabilizing compounds (left-side, Fig. 1). The injection of ions increased the *C*d of gas flow passing through the spark ablation passage between Ag or Cu rods, further stabilizing the generation of Ag or Cu particles. The Ag or Cu particles in the absence and presence of unipolar ion injection were finally collected to examine their antibacterial activities (*i.e.*, minimum inhibitory concentration [MIC] and antibacterial filter efficiency) and stabilities against *Escherichia coli* (*E. coli*; gram-negative) and *Staphylococcus epidermidis* (*S. epidermidis*; gram-positive), including MDR strains (right side, Fig. 1).

2. Experimental

2.1. Plug-in manufacture of ultrasmall Ag or Cu particles

2.1.1. Spark chamber

To ablate Ag or Cu metals, two identical Ag (AG-402651, Nilaco, Japan) or Cu (CU-112651, Nilaco, Japan) rods (*i.e.*, spark electrodes) were installed inside a polytetrafluoroethylene (PTFE) chamber (32 × 32 × 32 mm^3) with a gap distance of 0.3 mm. A carbon brush tip for carrier gas unipolar ionization was located 10 mm behind the spark ablation channel, as shown in Fig. S1.

2.1.2. Spark ablation

Two IGBT switches (*S1* and *S2*, IXBH12N300, IXYS, USA), a ceramic capacitor (1 nF, SV15JA102JAR, AVX, USA), and a high-voltage DC power supply (UltraVolt, USA) were connected to two identical Ag or Cu rods, as shown in Fig. S2A. Details of the IGBT switches and voltage waveforms are depicted in Figs. S2B and S2C, respectively. A bluish spark channel (> 4000 °C) was formed between Ag or Cu electrodes after plugging in the ablation system. This induced vaporization of a part of the electrodes, and the Ag or Cu vapors were condensed into Ag or Cu primary particles through a quenching effect using room temperature nitrogen gas (99.9999% purity) flow (5 L min^{-1}).

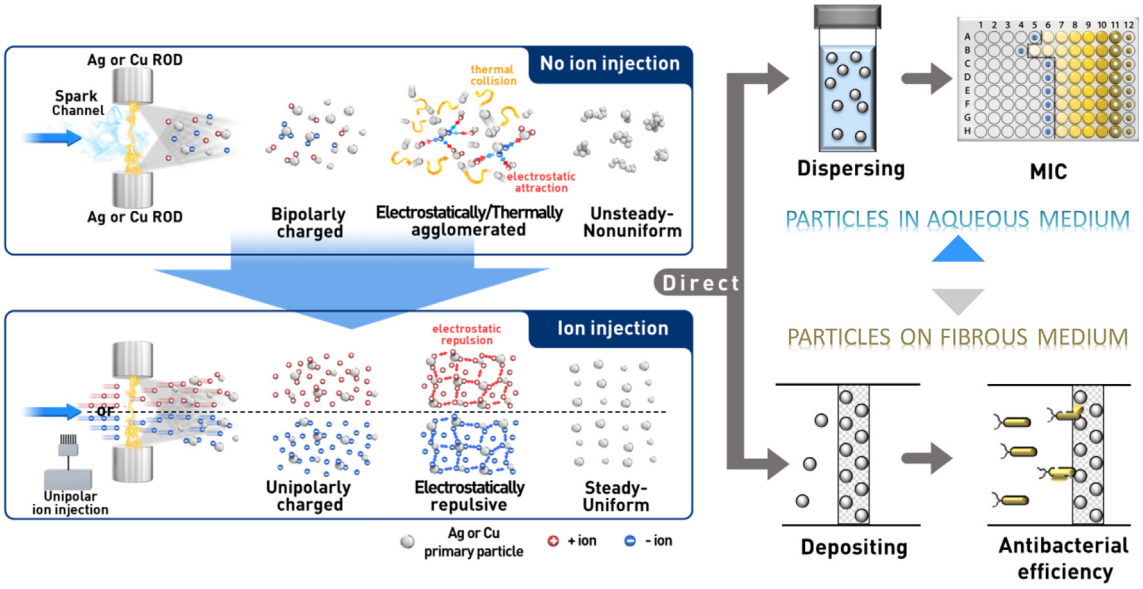

Fig. 1. Schematic of Ag or Cu particle manufacture using a tandem electrostatic system and successive evaluation of the particles for antibacterial activities. The antibacterial activities of Ag or Cu particles produced in the presence of unipolar ions (electrostatically repulsive configuration) were compared with particles produced in the absence of unipolar ions (existing thermal collision and/or electrostatic attraction between Ag or Cu particles). The produced particles were directly dispersed in buffered saline and deposited on fibrous medium to evaluate MICs and antibacterial filter efficiencies, respectively.

2.1.3. Positive or negative gaseous ion generation

A carbon brush ionizer (SJ-1000, Sejin Electronics, Republic of Korea) containing 200 ± 20 of carbon fibers (5–10 μm diameter as ionizing tips) and a rheostat-controlled power pack was selected to generate positive or negative gaseous ions. The ion concentration was controlled by modulating rheostat resistance, which was measured using an ion counter (AIC20M, AlphaLab, USA) under nitrogen gas flow of 5 L min^{-1}. The electrostatic polarity of the spark-produced particles was monitored using an aerosol electrometer (Charme®, Palas, Germany) during spark ablation in the absence and presence of unipolar ions (1×10^7 ions cm^{-3}), as shown in Fig. S2D.

2.1.4. Particle collection

For Ag or Cu particle dispersion, the particles produced in the presence of gas ions were electrostatically separated from the particle-laden flow on a polished stainless steel rod in an electric field ($\pm$ 0.8 kV cm^{-1}). The Ag or Cu particle-deposited rod was then immersed in buffered saline under bath sonication for 10 min, resulting in Ag or Cu dispersion. In the case of Ag or Cu particles produced in the absence of ion injection, a pin-to-ring type corona charger (+1.6 kV cm^{-1}) was used to unipolarly charge the particles, and the charged particles were collected on the stainless steel rod in an electric field (−0.8 kV cm^{-1}). A filter for testing antibacterial efficiency was prepared *via* mechanical filtration of spark produced Ag or Cu particles on a 4 × 4 cm^2 glass fiber medium (class for high-efficiency particulate air [HEPA] filter). The areal density of Ag or Cu particles was selected as 10 μg cm^{-2}, which was achieved by controlling the filtration time.

2.2. Characterization

2.2.1. Aerosol size distribution

Changes in the size distribution induced by injecting gaseous unipolar ions into the spark channel were examined using a SMPS (3936, TSI, USA) system. The system consisted of a soft X-ray charger (for securing the Boltzmann charge distribution), electrostatic classifier (for size classification), and condensation particle counter (for counting particle numbers), and the flow rates for sampling and guiding aerosol Ag or Cu particles were set at 0.3 and 3.0 L min^{-1}, respectively.

2.2.2. Morphology, size distribution, and microstructure

The morphology, size distribution, and microstructure of the produced Ag or Cu particles were observed using TEM (JEM-F200, JEOL, Japan). The specimens were prepared *via* the direct deposition of Ag or Cu aerosol particles onto a carbon-coated copper grid (Tedpella, USA) that was placed on a grid sampler (Ineris, France). ImageJ software was used to determine the size distribution of Ag or Cu singlet particles (N = 110) in the absence and presence of unipolar ions.

2.3. Bioassay

2.3.1. MIC evaluation

The MIC of the produced particles against the tested bacteria (gram-positive and gram-negative, including MDR bacteria) was determined using the broth microdilution method. The bacteria were seeded onto 96-well microtiter plates (SPL34096, SPL Life Sciences, Republic of Korea) containing tryptic soy broth (TSB) and Ag or Cu particles (with chosen concentrations) at 1×10^5 CFU mL^{-1} (in 100 μL). After 24 h incubation at 37 °C, the MIC was estimated against each strain.

2.3.2. Cell morphology

Morphological changes of the test bacteria were observed *via* SEM (JSM-7800F, JEOL, Japan) to confirm the antibacterial activity of the spark produced particles. The bacteria (1×10^5 CFU mL^{-1}) were incubated in TSB medium containing Ag or Cu particles (30 μg mL^{-1}) for 1 h at 37 °C. The treated bacteria were then washed and resuspended in deionized water, and a drop (5 μL) was placed on a silicon wafer (Tedpella, USA). The sample was dried in ambient air and treated in a vacuum platinum coater for SEM measurements.

2.3.3. Antibacterial filter test

To examine the antibacterial activity for airborne bacteria (*i.e.*, bioaerosols), the test bacteria were aerosolized using a commercial aerosol generator (3076, TSI, USA) at an air flow rate of 3 L min^{-1}. The bacteria-laden air flow passed through a Ag or Cu particle deposited glass fiber filter (10 μg [Ag or Cu] cm^{-2} [HEPA-grade glass fiber filter]) for 10 min to attach the airborne bacteria onto the surfaces of the filter. The filter was then immersed in buffered saline under bath sonication for 10 min to detach the bacteria from the filter. The bacterial solution

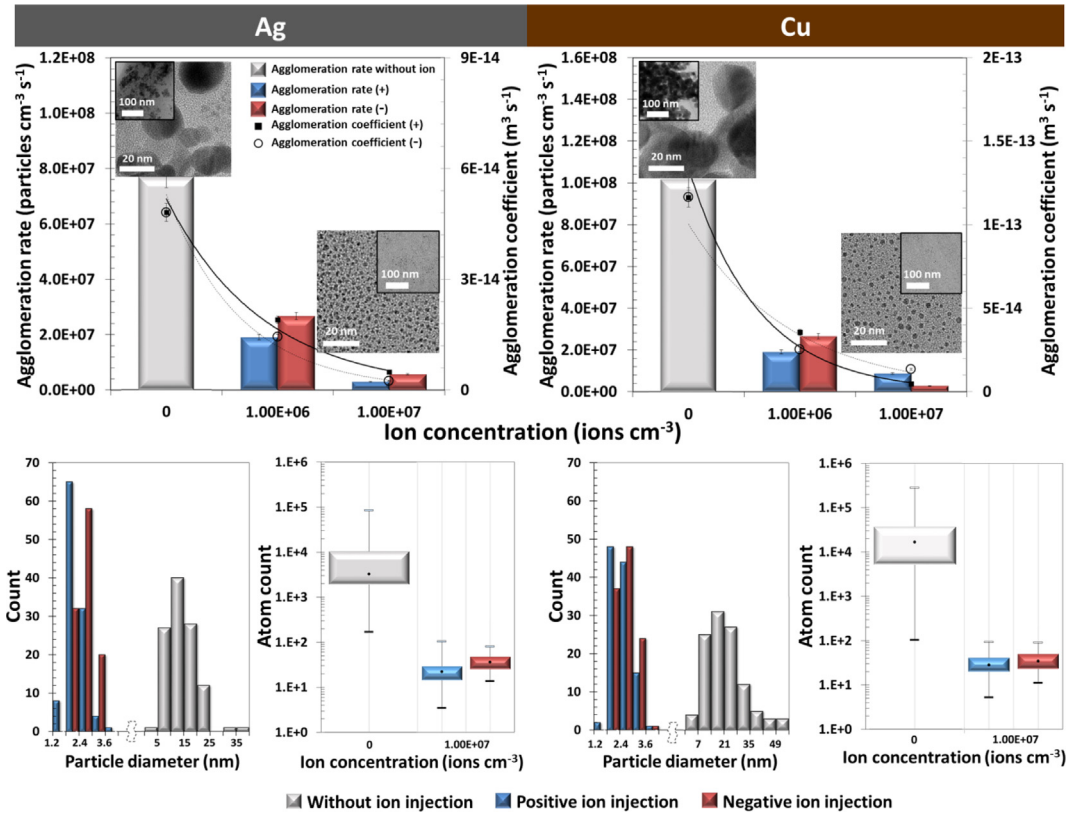

Fig. 2. Analytical and experimental evaluation of the anti-aggregation and anti-agglomeration activities of spark-produced Ag or Cu particles in the presence of unipolar ions. The upper two graphs show the agglomeration rate and coefficient of Ag or Cu particles produced in the absence and presence (1×10^6 and 1×10^7 ions cm^{-3}) of unipolar (positive and negative) ions. Inset, low- and high-magnification TEM images show the representative morphologies of Ag or Cu particles in the absence and presence (1×10^7 ions cm^{-3}) of unipolar ions. The lower images show the corresponding histograms and box plots of particle size distribution and atom count in the absence and presence of unipolar ions.

was spread on an agar plate after dilution and incubated for 24 at 37 °C. The antibacterial efficiencies were estimated by comparing the CFUs between the bacteria from clean and Ag- or Cu-deposited filters. Viable bacteria were indicated by green fluorescence and were visualized *via* CLSM (LSM 880, Carl Zeiss, Germany) to confirm the antibacterial activities of the particles.

3. Results and discussion

To verify the effect of ion injection on particle formation, the agglomeration rate ($dN[t]/dt$, particles $cm^{-3}\,s^{-1}$) and morphology (using transmission electron microscopy [TEM]) of spark-produced Ag or Cu particles were analytically estimated and experimentally observed in the absence and presence of unipolar gaseous ions (upper side of Fig. 2). The agglomeration rate was determined by estimating the change of the number concentration using the following formula [32]:

$$\frac{dN(t)}{dt} = -\frac{N_0^2 K}{(1 + N_0 K t)^2}$$

where N_0 is the initial particle number concentration, K is the agglomeration coefficient ($m^3\,s^{-1}$), and t is elapsed time (s), whereas the spark-produced particles (with and without unipolar ions) were directly deposited on a carbon-coated copper grid through mechanical impaction for TEM observation. By increasing ion concentration from 1×10^6 to 1×10^7 ions cm^{-3}, the agglomeration coefficient decreased exponentially, resulting in significant decreases of the agglomeration rate. There were no significant differences in the rate between both ion polarities (positive and negative) and particle species (Ag and Cu), implying that creating a unipolar condition near the spark channel is a critical parameter for suppressing agglomeration between the produced particles. Low- and high-magnification inset TEM images (also shown in Fig. S3) for without and with gaseous ions (1×10^7 ions cm^{-3}) revealed physical (electrostatic) suppression of the agglomeration between singlet (primary) Ag or Cu particles. The particle size distributions of Ag and Cu particles analyzed using ImageJ software demonstrated no overlaps between the configurations (without and with gaseous ions, lower side of Fig. 2), revealing significant differences in the atom count of singlet Ag or Cu particles between the configurations, as summarized in Table S1. In the case of ion injection, the spherical singlet Ag or Cu particles were well isolated with sizes smaller than 3 nm (*i.e.*, ultrasmall) because of high concentration unipolar (positive or negative) ions surrounding the metal particles or vapors (to be condensed into particles) that facilitated the formation of atomically countable (< 40 atoms, estimated *via* the following equation: $N_{atom} = V_p/V_{unit\ cell} = \pi R_p{}^3/0.2023$, where V_p, $V_{unit\ cell}$, and R_p are the particle volume [nm^3], unit cell volume of a fcc crystal [nm^3], and particle radius [nm], respectively) Ag or Cu structures in the gas phase. Conversely, agglomerated (or aggregated) structures were found in the absence of unipolar ions because of thermal collision and electrostatic attraction (because of its bipolar nature, Fig. S2D) between singlet particles (or vapors), as shown in other inset TEM images. Fig. S3 shows the representative lattice fringes of the spark-produced Ag or Cu particles in the absence and presence of unipolar ions. There were no differences in *d*-spacing values (0.234 nm for Ag and 0.213 nm for Cu assigning to [1 1 1] plane of fcc Ag and Cu, respectively) between the presence and absence of unipolar ions, suggesting that ion injection did not affect the crystallinity of the Ag or Cu particles. The aerosol size distributions of Ag or Cu particles (Fig. S4 and Table S2) measured using a scanning mobility particle sizer (SMPS) did not exhibit significant differences in the geometric mean diameter (GMD) and

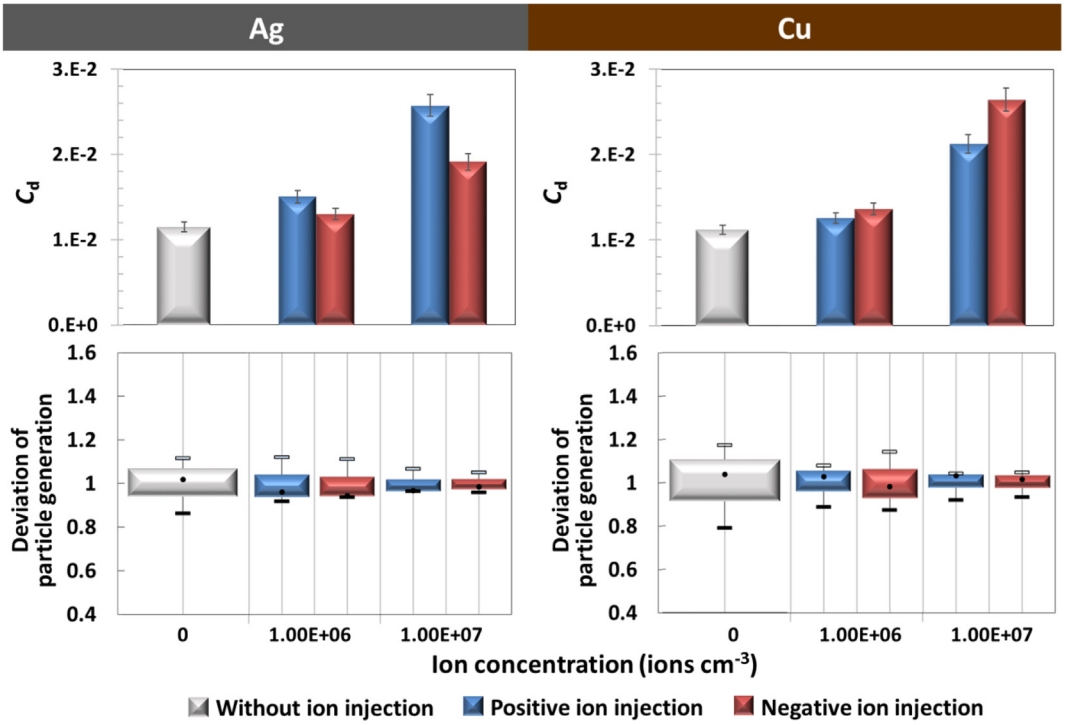

Fig. 3. Analytical and experimental evaluation of the stabilities of gas flow and particle generation in the absence and presence of unipolar ions. The upper two graphs show the C_d of gas flow passing through the spark ablation (Ag or Cu) passage. The lower two box plots show the deviation of Ag or Cu particle generation, which were monitored using a SMPS. The monitored items (particle concentration and diameter) are displayed in Fig. S6.

geometric standard deviation (GSD) between the presence and absence of unipolar ions because the measurement included an electrostatic charge neutralization process (eliminating highly unipolar charges from the ion injection to ensure electrostatic size classification) that altered the electrostatic status of Ag or Cu particles from repulsive to agglomerative. This thus induced notable discrepancies in size distributions between TEM and SMPS (~23 nm for Ag and ~26 nm for Cu at 1×10^7 ions cm^{-3}) measurements, although there were slight decreases in the GMD for ion injection compared with no ion injection, proving a key role of unipolar ion injection in securing uniform distribution of the singlet particles.

Regarding particle generation stability, the C_d of gas flow passing through the spark ablation passage between Ag or Cu rods and deviation of particle generation were analytically estimated and experimentally examined in the absence and presence of unipolar gaseous ions (Fig. 3). The C_d was determined by applying the electrostatic pressure difference (Pa) ($\Delta P = [\varepsilon_0/2]\ [V_s - V_{avg}/d]^2$, where ε_0 is the vacuum permittivity [F m^{-1}], d is the gap distance between Ag or Cu rods [m], and V_s and V_{avg} are individual and averaged sparking voltages [V], respectively) using the following formula [36–38]:

$$C_d = \frac{Q}{A\sqrt{2\rho\Delta P}}$$

where Q is the mass flow rate of gas (kg s^{-1}), A is the cross-sectional area of flow passage (m^2), and ρ is the density of gas (kg m^{-3}). As shown in Fig. S5, V_s approached V_{avg} when the unipolar ion concentration was increased, and the waveform of the voltage in the presence of unipolar ions was more uniform than that in the absence of ion injection. This may be attributable to the higher densities of unipolar ions at the spark ablation passage, which facilitates the formation of abundant conductive channels (representing reduction of sparking voltage) by minimizing dielectric spots (deriving overvoltage peaks through dielectric breakdown) at the passage. C_d values were thus increased by increasing the concentration of unipolar ions regardless of the metal species, and there were no significant differences in ion polarity, similar to the results (unipolar ion concentration-dependent) depicted in Fig. 2. This suggests that the decrease in ΔP between the entrance and exit of the ablation passage caused by decreasing the difference between V_s and V_{avg} can make Q stable at the passage similarly as the choking flow to minimize fluctuation of Q passing through a nozzle or an orifice [39]. The deviation of the particle generation rate examined using SMPS (lower-side of Fig. 3) further supported the increases of C_d caused by increasing the ion concentration, after which the Ag or Cu particles produced in the presence of unipolar ions were more stably discharged from the passage. The monitored particle concentrations (mass and number) and mode diameters after 30 min of spark ablation using SMPS are shown in Fig. S6. Ion injection reduced the dynamic range of the concentrations and diameters during the operation, proving that the combination of unipolar ion injection and spark ablation can provide a suitable platform, even for the stable plug-in manufacture of Ag or Cu particles, without complex controls. This anti-agglomeration effect was also examined for the spark production of Mg or Zn particles, as shown in Fig. S7. The unipolar ion injection was workable to significantly suppress agglomeration of the particles, suggesting extendability of the developed system for other metallic particles.

The antibacterial activities of spark produced Ag or Cu particles in the absence and presence of unipolar ions were examined by estimating MICs and antibacterial efficiencies for *E. coli* and *S. epidermidis* after the particles were directly dispersed in buffered saline and deposited on the surfaces of fibrous filter medium, respectively (Fig. 4). The mass (mg) of Ag or Cu particles was estimated by calculating the average particle generation rate (μg min^{-1}, calculated using SMPS data), collection time (min), and collection efficiency (η [D_p], where D_p is the equivalent mobility particle diameter) to evaluate the dynamic range of antibacterial activity. *S. epidermidis* was linked to larger MICs both for Ag and Cu particle treatments, which may be relevant to the stronger resistance to the particles because of the bacterium's thicker and more complex peptidoglycan layers [40,41]. The stronger inhibitory activities of Ag relative to Cu may be attributable to the lower bond

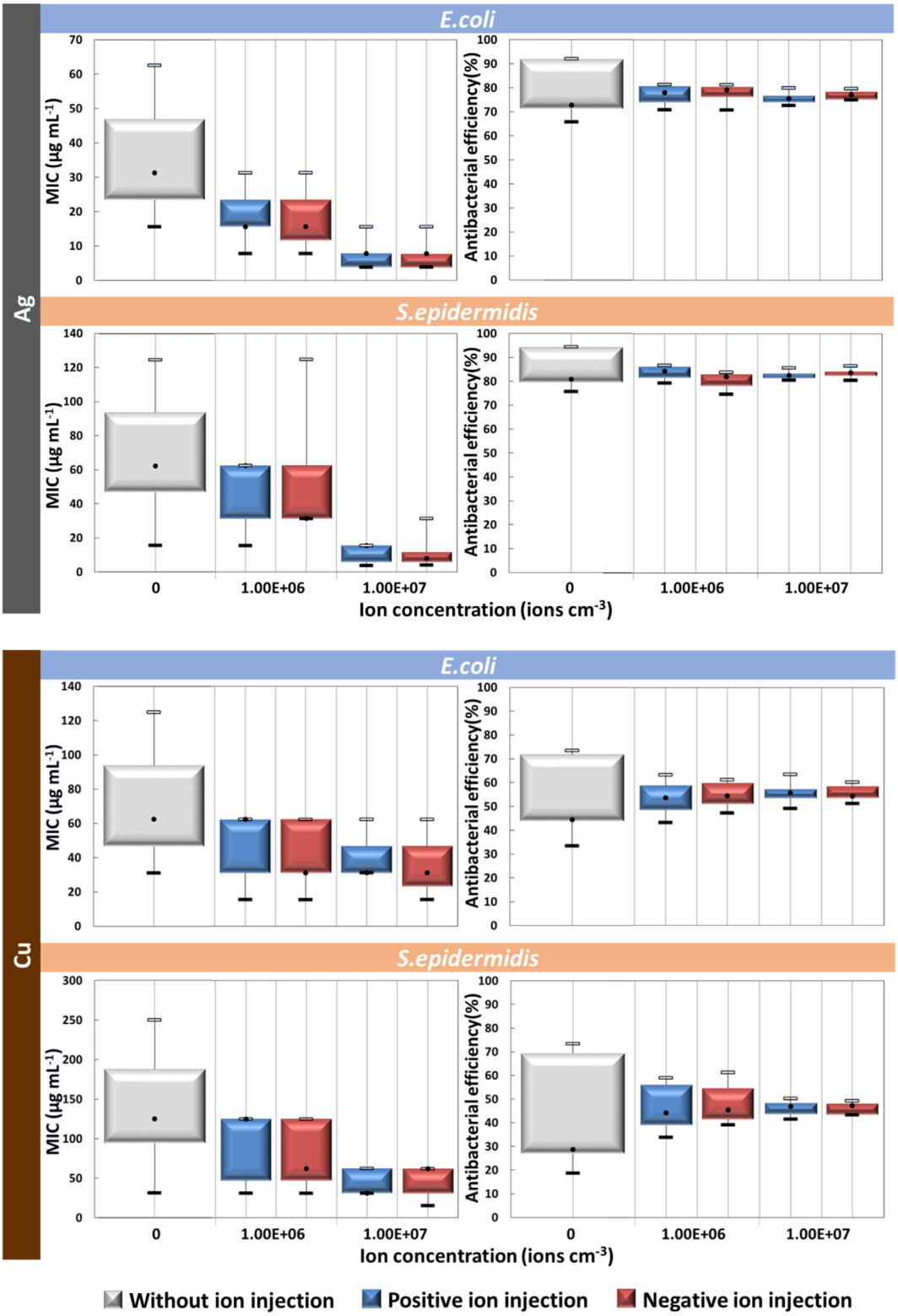

Fig. 4. MICs and antibacterial filter efficiencies of spark-produced Ag or Cu particles in the absence and presence of unipolar ions for *E. coli* and *S. epidermidis*. The upper and lower box plots show the results for Ag and Cu applications, respectively. The applied particle concentration (MIC) and deposition intensity (antibacterial efficiency) were calculated using the average particle generate rate (measured using a SMPS) of each generation configuration (no ions, 1×10^6 and 1×10^7 ions cm^{-3}). The antibacterial efficiency was estimated for *E. coli* and *S. epidermidis* bioaerosols after their collection on the Ag or Cu particle-deposited fibrous filter medium.

dissociation energy of Ag–Ag than of Cu–Cu [42]. The lower MICs for bacteria treated with particles produced in the presence of unipolar ions may be caused by their smaller sizes (deriving greater Ag or Cu release rate [$\mu g\,cm^{-2}\,h^{-1}$]) according the following formula [43]:

$$r_{release} = \frac{c_p V_p}{m_s SSA t_{exp}}$$

where c_p is the particle concentration ($\mu g\,L^{-1}$), m_s is the sample mass (g), *SSA* is the specific surface area ($cm^2\,g^{-1}$), and t_{exp} is the exposure time (h). The Ag or Cu particles produced in the presence of 1×10^7 ions cm^{-3} (*i.e.*, ultrasmall particles) can facilitate approximately 38- or 73-fold greater $r_{release}$, respectively, when only the particle size is arithmetically considered for the rate estimation. Contrarily, the ultrasmall particles exhibited only 2–7-fold lower MICs, which might be due to the exponential increase of the core and valence binding energies of Ag or Cu particles induced by decreasing their size [44,45]. The decrease in size *via* unipolar ion injection thus provided more sustained release of Ag or Cu to deactivate bacterial growth. Nevertheless, the Ag or Cu particles exhibited significantly lower MICs compared with previous studies, as summarized in Table S3, representing the importance of ultrasmall sizes for antibacterial activity. In the antibacterial filter test, the ultrasmall particles did not exhibit stronger activities, demonstrating comparable efficiencies with those of particles produced in the absence of unipolar ions. This may be due to the different collection mechanisms of aerosolized bacteria (> 1 μm) and aerosol Ag or Cu particles (< 50 nm). According to the aerosol collection theory of fibrous medium, impaction and interception of the bacteria on the outermost surface of fibrous medium were the governing collection mechanisms, whereas Brownian diffusion of Ag or Cu particles onto the surface of the medium (depth filtration) governed the collection [46]. Diffusional motion of the particles is inversely proportional to particle size; thus, the ultrasmall particles (< 4 nm) were more capable of depth filtration than the particles (< 50 nm) produced in the absence of unipolar ions. This may reduce the frequency of direct contact between the bacteria and ultrasmall particles at the outermost surface of the medium, resulting in comparable antibacterial efficiencies. Nevertheless, the differences in antibacterial efficiency between Ag and Cu were consistent with the MIC measurements, suggesting that bond dissociation energy is also valid for assessing the activities deactivating aerosolized bacteria on fibrous medium.

Scanning electron microscopy (SEM) and confocal laser scanning microscopy (CLSM) were further used to observe morphological changes and cell viability, respectively. The SEM images of untreated and treated bacteria exhibited significant morphological differences (Fig. 5); in particular, irreversible distortion of the treated strains was probably due to the impaired membrane functions because of interactions between the bacteria and particles [47]. In addition, survival of Ag or Cu particles after exposure to the strains was examined by TEM observation of the extracts from particle-bacteria media, as shown in Fig. S8. Tiny black dots (Ag or Cu particles) were still distributed along with grayish blurs, proving sustained release of Ag^+ or Cu^{2+} ions because of their strong core and valence binding energies [44,45]. The generation of red (dead; green: live) fluorescent dots in the CLSM observation after the particle treatments further supported the bacterial cell damage caused by the interactions. These observations were further conducted for MDR strains (*i.e.*, extended-spectrum beta-lactamase [ESBL]-producing *E. coli* [gram-negative] and methicillin-resistant *Staphylococcus aureus* [MRSA, gram-positive]) after the particle treatments to assess the extendability of the ultrasmall Ag or Cu particles. The insets of Fig. 6 (SEM images) and S9 (CLSM images) illustrate the comparable results with those for *E. coli* and *S. epidermidis*, proving the effectiveness of the ultrasmall particles in deactivating MDR strains. The larger MICs for gram-negative strains, lower MICs for Ag particle treatments, and comparable filter efficiencies between the particles in the absence and presence of unipolar ions were also consistent with results depicted in Fig. 4, and the ultrasmall particles also exhibited lower deviations in the MIC evaluation and antibacterial filter test. These findings collectively suggest that employing the tandem electrostatic system as a base manufacture platform for supplying ultrasmall (atomically countable) Ag or Cu particles may be a realizable strategy for ensuring stronger and more stable (precision) functions for a wide range of antibacterial applications.

4. Conclusions

The tandem electrostatic system developed in this study was feasible for manufacturing uniform ultrasmall (atomically countable, ~40 atoms) Ag or Cu particles in a continuous-flow manner. The injection of unipolar (positive or negative) gaseous ions (1×10^7 ions cm^{-3}) into the spark ablation passage between Ag or Cu rods both ensured an electrostatically repulsive environment to suppress agglomeration between singlet Ag or Cu particles and enhanced the C_d of gas flow passing through the passage during spark ablation, resulting in the stable manufacture of ultrasmall Ag (2.29 ± 0.42 nm with positive ions; 2.63 ± 0.40 nm with negative ions) or Cu (2.51 ± 0.46 nm with positive ions; 2.64 ± 0.46 nm with negative ions) particles. These Ag or Cu particles had > 4-fold lower MICs for *E. coli* (or 2-fold lower for *S. epidermidis*) than the particles produced in the absence of unipolar ions, and this tendency was consistent for MDR strains. Because of the smaller deviations in particle generation, the particles generated in the presence of unipolar ions exhibited significantly narrower fluctuations in both MIC (fewer than half) and antibacterial filter efficiency (fewer than one-fifth), suggesting that the tandem system is suitable for ensuring stronger and more stable antibacterial activities as a plug-in platform. These findings both offer a practical strategy for continuously manufacturing ultrasmall particles without wet chemical processes and

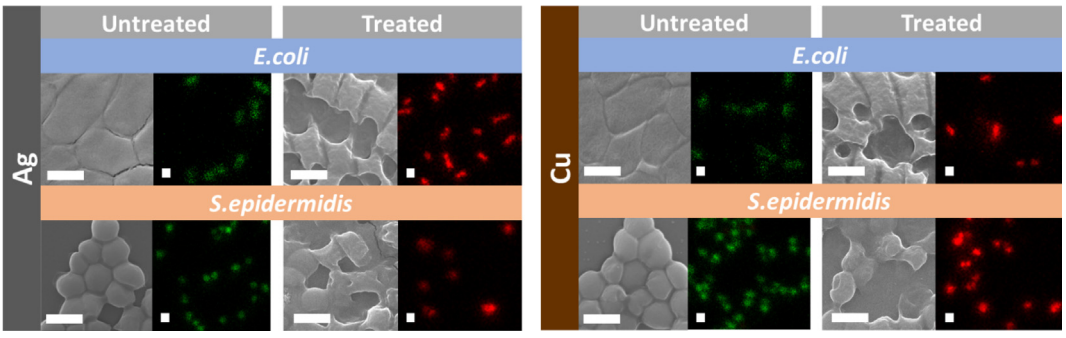

Fig. 5. SEM and CLSM observation of *E. coli* and *S. epidermidis* treated with spark produced Ag (left) or Cu (right) particles (at 30 μg mL^{-1}) in the presence of unipolar ions (1×10^7 ions cm^{-3}). The SEM images reveal morphological differences between the untreated and treated bacteria, whereas the CLSM images reveal differences in fluorescence between the untreated (green: live) and treated (red: dead) bacteria. Scale bars, 1 μm. (For interpretation of the references to colour in this figure legend, the reader is referred to the web version of this article.)

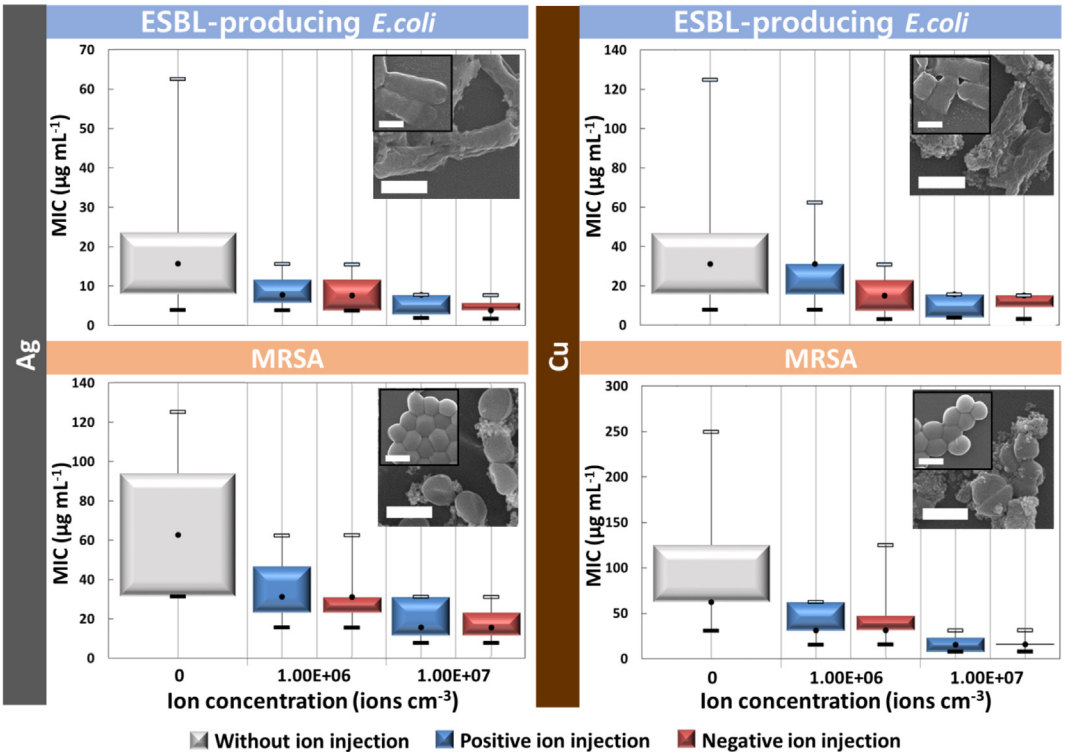

Fig. 6. Box plots of the MICs and dynamic range for EBSL-producing E. coli and MRSA treated with spark-produced Ag or Cu particles in the absence and presence of unipolar ions. Insets show the representative SEM images (scale bar, 1 μm) of each strain without and with Ag or Cu particles. These tests were conducted to confirm the extendability of the tandem electrostatic system for deactivating MDR strains.

provide a base technology for realizing on-demand, precision, sustained, safe, and broad-spectrum antibacterials *via* integration with dispensing systems for pre- or post-functionalization of the ultrasmall particles.

Acknowledgements

This research was supported by Basic Science Research Program through the National Research Foundation of Korea (NRF) funded by the Ministry of Science, ICT and future Planning (NRF-2018R1A2A1A05020683).

Appendix A. Supplementary data

Supplementary data to this article can be found online at https://doi.org/10.1016/j.cej.2019.122639.

References

[1] B. Hu, C. Owh, P.L. Chee, W.R. Leow, X. Liu, Y.-L. Wu, P. Guo, X.J. Loh, X. Chen, Supramolecular hydrogels for antimicrobial therapy, Chem. Soc. Rev. 47 (2018) 6917–6929.
[2] C.N. Spaulding, R.D. Klein, H.L. Schreiber IV, J.W. Janetka, S.J. Hultgren, Precision antimicrobial therapeutics: the path of least resistance, NPJ Biofilms Microbiomes 4 (2018) 4.
[3] C. de la Fuente-Nunez, M.D.T. Torres, F.J.M. Mojica, T.K. Lu, Next-generation precision antimicrobials: Towards personalized treatment of infectious diseases, Curr. Opin. Microbiol. 37 (2017) 95–102.
[4] C. Xue, X. Song, M. Liu, F. Ai, M. Liu, Q. Shang, X. Shi, F. Li, X. He, L. Xie, T. Chen, H. Xin, X. Wang, A highly efficient, low-toxic, wide-spectrum antibacterial coating designed for 3D printed implants with tailorable release properties, J. Mater. Chem. B 5 (2017) 4128–4136.
[5] T. Wei, Z. Tang, Q. Yu, H. Chen, Smart antibacterial surfaces with switchable bacteria-killing and bacteria-releasing capabilities, ACS Appl. Mater. Interfaces 9 (2017) 37511–37523.
[6] G. Gao, Y.-W. Jiang, H.–R. Jia, F.–G. Wu, Near-infrared light-controllable on-demand antibiotics release using thermo-sensitive hydrogel-based drug reservoir for combating bacterial infection, Biomaterials 188 (2019) 83–95.
[7] S. Rigo, C. Cai, G. Gunkel-Grabole, L. Maurizi, X. Zhang, J. Xu, C.G. Palivan, Nanoscience-based strategies to engineer antimicrobial surfaces, Adv. Sci. 5 (2018) 1700892.
[8] Y.N. Slavin, J. Asnis, U.O. Häfeli, H. Bach, Metal nanoparticles: Understanding the mechanisms behind antibacterial activity, J. Nanobiotechnol. 15 (2017) 65.
[9] M.I. Din, F. Arshad, Z. Hussain, M. Mukhtar, Green adeptness in the synthesis and stabilization of copper nanoparticles: catalytic, antibacterial, cytotoxicity, and antioxidant activities, Nanoscale Res. Lett. 12 (2017) 638.
[10] K.B.A. Ahmed, T. Raman, A. Veerappan, Future prospects of antibacterial metal nanoparticles as enzyme inhibitor, Mater. Sci. Eng. C 68 (2016) 939–947.
[11] L. Tamayo, M. Azócar, M. Kogan, A. Riveros, M. Páez, Copper–polymer nanocomposites: an excellent and cost-effective biocide for use on antibacterial surfaces, Mater. Sci. Eng. C 69 (2016) 1391–1409.
[12] K. Simeonidis, S. Mourdikoudis, E. Kaprara, M. Mitrakas, L. Polavarapu, Inorganic engineered nanoparticles in drinking water treatment: a critical review, Environ. Sci.: Water Res. Technol. 2 (2016) 43–70.
[13] J. Ren, P. Han, H. Wei, L. Jia, Fouling-resistant behavior of silver nanoparticle-modified surfaces against the bioadhesion of microalgae, ACS Appl. Mater. Interfaces 6 (2014) 3829–3838.
[14] K. Blecher, A. Nasir, A. Friedman, The growing role of nanotechnology in combating infectious disease, Virulence 2 (2011) 395–401.
[15] D.N. Williams, S.H. Ehrman, T.R.P. Holoman, Evaluation of the microbial growth response to inorganic nanoparticles, J. Nanobiotechnol. 4 (2006) 3.
[16] H. Kong, J. Jang, Antibacterial properties of novel poly(methyl methacrylate) nanofiber containing silver nanoparticles, Langmuir 24 (2008) 2051–2056.
[17] Y. Su, L. Zhao, F. Meng, Q. Wang, Y. Yao, J. Luo, Silver nanoparticles decorated lipase-sensitive polyurethane micelles for on-demand release of silver nanoparticles, Colloids Surf. B Biointerfaces 152 (2017) 238–244.
[18] T. Dai, C. Wang, Y. Wang, W. Xu, J. Hu, Y. Cheng, A nanocomposite hydrogel with potent and broad-spectrum antibacterial activity, ACS Appl. Mater. Interfaces 10 (2018) 15163–15173.
[19] P. Pallavicini, B. Bassi, G. Chirico, M. Collini, G. Dacarro, E. Fratini, P. Grisoli, M. Patrini, L. Sironi, A. Taglietti, M. Moritz, I. Sorzabal-Bellido, A. Susarrey-Arce, E. Latter, A.J. Beckett, I.A. Prior, R. Raval, Y.A.D. Fernandez, Modular approach for bimodal antibacterial surfaces combining photo-switchable activity and sustained biocidal release, Sci. Rep. 7 (2017) 5259.
[20] W. Shao, H. Liu, X. Liu, H. Sun, S. Wang, R. Zhang, pH-responsive release behavior and anti-bacterial activity of bacterial cellulose-silver nanocomposites, Int. J. Biol. Macromol. 76 (2015) 209–217.
[21] B.K. Poudel, J.H. Park, J.H. Byeon, On-demand gas-to-liquid process to fabricate thermoresponsive antimicrobial nanocomposites and coatings, ACS Appl. Mater. Interfaces 9 (2017) 15342–15349.
[22] M.-S. Wong, C.–W. Chen, C.–C. Hsieh, S.–C. Hung, D.–S. Sun, H.–H. Chang, Antibacterial property of Ag nanoparticle-impregnated N-doped titania films under visible light, Sci. Rep. 5 (2015) 11978.
[23] M. Chang, W.-S. Lin, W. Xiao, Y.–N. Chen, Antibacterial effects of magnetically-

controlled Ag/Fe_3O_4 nanoparticles, Materials 11 (2018) 659.
[24] F. Cavalieri, L. Micheli, S. Kaliappan, B.M. Teo, M. Zhou, G. Palleschi, M. Ashokkumar, Antimicrobial and biosensing ultrasound-responsive lysozyme-shelled microbubbles, ACS Appl. Mater. Interfaces 5 (2013) 464–471.
[25] R. Tian, X. Qiu, P. Yuan, K. Lei, L. Wang, Y. Bai, S. Liu, X. Chen, Fabrication of self-healing hydrogels with on-demand antimicrobial activity and sustained biomolecule release for infected skin regeneration, ACS Appl. Mater. Interfaces 10 (2018) 17018–17027.
[26] R.I. MacCuspie, A.J. Allen, M.N. Martin, V.A. Hackley, Just add water: Reproducible singly dispersed silver nanoparticle suspensions on-demand, J. Nanopart. Res. 15 (2013) 1760.
[27] S. Yan, H. Shi, L. Song, X. Wang, L. Liu, S. Luan, Y. Yang, J. Yin, Nonleaching bacteria-responsive antibacterial surface based on a unique hierarchical architecture, ACS Appl. Mater. Interfaces 8 (2016) 24471–24481.
[28] F. Paladini, M. Pollini, A. Sannino, L. Ambrosio, Metal-based antibacterial substrates for biomedical applications, Biomacromolecules 16 (2015) 1873–1885.
[29] B.K. Poudel, K.-O. Doh, J.H. Byeon, Ag photoionization-induced single-pass assembly of Ag_2S nanodots in flowing thiol droplets, Green Chem. 20 (2018) 978–983.
[30] J.H. Byeon, Scalable hybrid chemical manufacture to photothermal therapy: PEG-capped phototransducers, Sci. Rep. 6 (2016) 31351.
[31] A. Nikiforov, X. Deng, Q. Xiong, U. Cvelbar, N. DeGeyter, R. Morent, C. Leys, Non-thermal plasma technology for the development of antimicrobial surfaces: a review, J. Phys. D. Appl. Phys. 49 (2016) 204002.
[32] J. Feng, G. Biskos, A. Schmidt-Ott, Toward industrial scale synthesis of ultrapure singlet nanoparticles with controllable sizes in a continuous gas-phase processes, Sci. Rep. 5 (2015) 15788.
[33] K. Zheng, M.I. Setyawati, D.T. Leong, J. Xie, Antimicrobial silver nanomaterials, Coord. Chem. Rev. 357 (2018) 1–17.
[34] M.D. Susman, Y. Feldman, A. Vaskevich, I. Rubinstein, Chemical deposition of Cu_2O nanocrystals with precise morphology control, ACS Nano 8 (2014) 162–174.
[35] J.B. Liu, M.X. Yu, C. Zhou, J.J. Zheng, Renal clearable inorganic nanoparticles: a new frontier of bionanotechnology, Mater. Today 16 (2013) 477–486.
[36] D.A. Jobson, On the flow of a compressible fluid through orifices, Proc. Inst. Mech. Eng. 169 (1955) 767–776.
[37] S.L. Bragg, Effect of compressibility on the discharge coefficient of orifices and convergent nozzles, J. Mech. Eng. Sci. 2 (1960) 35–44.
[38] M.R. Halder, S.K. Dash, S.K. Som, A numerical and experimental investigation on the coefficients of discharge and the spray cone angle of a solid cone swirl nozzle, Exp. Therm. Fluid Sci. 28 (2004) 297–305.
[39] H.J. Yoon, M. Ishii, S.T. Revankar, Choking flow modeling with mechanical and thermal non-equilibrium, Int. J. Heat Mass Transf. 49 (2006) 171–186.
[40] H.Y. Chang, J. Cang, P. Roy, H.T. Chang, Y.C. Huang, C.C. Huang, Synthesis and antimicrobial activity of gold/silver–tellurium nanostructures, ACS Appl. Mater. Interfaces 6 (2014) 8305–8312.
[41] J.S. Kim, E. Kuk, K.N. Yu, J.H. Kim, S.J. Park, H.J. Lee, S.H. Kim, Y.K. Park, Y.H. Park, C.-Y. Hwang, Y.K. Kim, Y.S. Lee, D.H. Jeong, M.H. Cho, Antimicrobial effects of silver nanoparticles, Nanomed. Nanotechnol. 3 (2007) 95–101.
[42] Y.-R. Luo, Comprehensive Handbook of Chemical Bond Energies, CRC Press, Boca Raton, FL, 2007.
[43] J. Hedberg, S. Skoglund, M.-E. Karlsson, S. Wold, I.O. Wallinder, Y. Hedberg, Sequential studies of silver released from silver nanoparticles in aqueous media simulating sweat, laundry detergent solutions and surface water, Environ. Sci. Technol. 48 (2014) 7314–7322.
[44] B. Balamurugan, T. Maruyama, Inhomogeneous effect of particle size on core-level and valence-band electrons: Size-dependent electronic structure of C_u3N nanoparticles, Appl. Phys. Lett. 89 (2006) 033112.
[45] I. Aruna, B.R. Mehta, L.K. Malhotra, S.M. Shivaprasad, Size dependence of core and valence binding energies in Pd nanoparticles: Interplay of quantum confinement and coordination reduction, J. Appl. Phys. 104 (2008) 064308.
[46] J.H. Park, K.Y. Yoon, K.C. Noh, J.H. Byeon, J. Hwang, Removal of PM2.5 entering through the ventilation duct in an automobile using a carbon fiber ionizer-assisted cabin air filter, J. Aerosol Sci. 41 (2010) 935–943.
[47] J.A. Lemire, J.J. Harrison, R.J. Turner, Antimicrobial activity of metals: Mechanisms, molecular targets and applications, Nat. Rev. Microbiol. 11 (2013) 371–384.